Diffusion and Diffusion-Controlled Kinetics during Epoxy–Amine Cure

Yong Deng and George C. Martin*

Department of Chemical Engineering and Materials Science, Syracuse University, Syracuse, New York 13244

*Received March 20, 1994; Revised Manuscript Received June 3, 1994**

ABSTRACT: The molecular diffusion and the diffusion-controlled kinetics during curing of an epoxy–amine resin have been studied. The diffusivity was estimated using an approach based on the dielectric analysis of the resin system. At low conversions, the decline of the diffusion coefficient is relatively slow while, at higher conversions, the diffusivity drops significantly even with a small advancement of cure. The normalized diffusion coefficient was in agreement with the predictions of the free-volume model of Huguenin and Klein but disagrees with those of the cooperative rearrangement model of Havlíček and Dušek. This discrepancy was attributed to an assumption of the cooperative rearrangement model. Based on the Rabinowitch model and the diffusion coefficient obtained, a diffusion-controlled kinetic model has been developed which accounts for the diffusional limitations on the cure kinetics and adequately predicts the experimental conversion profiles even at high conversions.

Introduction

The ultimate properties of thermosetting polymers are attained at the final stages of cure when the cross-linking reactions are limited by diffusion of the molecular species in the curing systems. To optimize the processing conditions, it is of practical importance to delineate the cure-dependent diffusion phenomena. Epoxy–amine resins are typical thermosetting polymers and have been widely used as structural and insulating materials. The major curing reactions of epoxy–amine resins are the addition of a primary or secondary amine with an epoxide to yield a hydroxyl group and a secondary or tertiary amine.[1,2] Although the rate constants for the reaction with primary amine and the reaction with secondary amine are not exactly the same,[3] it is often insignificant to distinguish between them.[2,4] The reactions are autocatalytic with proton donors as the catalyst.[5] The rate of reaction may be written as[2]

$$d\alpha/dt = (k_p\alpha + k_i)(1 - \alpha)(r - \alpha) \quad (1)$$

where α is the epoxide conversion, k_p is the intrinsic rate constant, k_i is the rate constant due to the catalysis of the impurity proton donors, r is the stoichiometric ratio (number of amine hydrogens/number of epoxides), and t is the time.

The objective of the present work was to characterize the cure-dependent diffusion of an epoxy–amine resin using a newly developed modeling approach[6] and to examine the diffusion-controlled reaction kinetics. The ionic conductivity and dipole relaxation time of the resin were first obtained from dynamic dielectric analysis and the molecular diffusion coefficient was estimated.[6] Then the diffusion coefficient was compared to the predictions of two existing models: the free-volume model of Huguenin and Klein[7] and the cooperative rearrangement model of Havlíček and Dušek.[8] Finally, the Rabinowitch model[9] for small-molecule reactions was employed to examine the diffusion-controlled kinetics of the epoxy resin.

Experimental Section

The epoxy resin used in this study was highly purified DGEBA (diglycidyl ether of Bisphenol A) supplied by the Shell Development Co. under the trade name X-22. The epoxide equivalent weight, as determined by titrating with hydrogen bromide in glacial acetic acid,[10] was 172 g/mol, which corresponds to a purity of 99%. 4,4′-Diaminodiphenylmethane (DDM), provided by Aldrich with 99% purity, was used as the amine cross-linking agent. The samples were prepared by melting the epoxy at 70 °C, cooling to 55 °C, and then adding a stoichiometrically balanced amount of the diamine. The mixture was mechanically stirred at a high speed for 15 min, when it became clear and transparent, and was then cooled and stored at −21 °C.

The curing kinetics of the resin was studied using an IBM Instruments IR/32S FTIR (Fourier transform infrared spectroscopy) spectrometer. In each experiment, the sample holder was first heated to slightly higher than the cure temperature. Then the liquid sample between a pair of NaCl cells was placed in the holder. The cell temperature reached the cure temperature in less than 2 min, and the infrared scans were initiated when the cell temperature was 2 °C below the cure temperature. Each IR spectrum consists of 15 coadded interferograms at 2 cm^{-1} resolution. The disappearance of the epoxide peak at 916 cm^{-1} was monitored and the aromatic ring–carbon–aromatic ring stretch at 1184 cm^{-1} was chosen as the reference peak. The epoxide conversion was then calculated using the following equation:

$$\alpha = 1 - \frac{A_{916}(t)\, A_{1184}(0)}{A_{916}(0)\, A_{1184}(t)} \quad (2)$$

where A_{916} is the area of the epoxide peak at 916 cm^{-1} and A_{1184} is the area of the reference peak at 1184 cm^{-1}.

A Mettler DSC-30 differential scanning calorimeter (DSC) was used to determine the glass transition temperature of the resin at various stages of cure. In each DSC test, an approximately 10 mg sample was first placed in an aluminum pan, cured isothermally for a period of time, cooled to −70 °C, and then scanned at a heating rate of 10 °C/min. The temperature corresponding to the onset of the endothermic deflection of the baseline was taken as the glass transition temperature of the sample.

Dielectric experiments were performed using a Micromet Eumetric System II microdielectrometer. When equipped with a low conductivity sensor, the dielectrometer can generate measurement signals ranging from 10000 to 0.005 Hz. Two types of isothermal experiments—curing experiments and frequency-scan tests—were conducted. In a curing experiment, the oven containing the dielectric sensor was heated to the cure temperature and a small amount of sample was used to cover the entire sensing area. While the cure proceeded, the sample was scanned repeatedly by the dielectrometer from high to low frequencies between 10000 and 0.01 Hz.

The frequency-scan tests were conducted to measure the ionic conductivity and dipole relaxation time of the pregel samples. Because these samples have relatively short relaxation times,

* Abstract published in *Advance ACS Abstracts*, July 15, 1994.

0024-9297/94/2227-5147$04.50/0

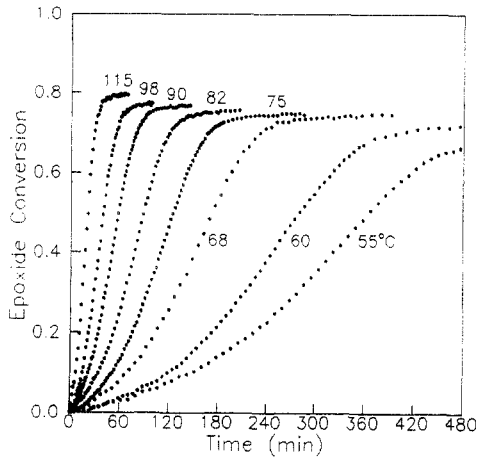

Figure 1. Epoxide conversion measured with FTIR at various cure temperatures.

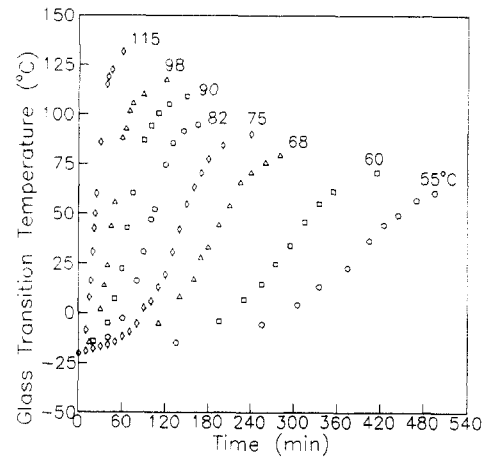

Figure 2. Glass transition temperature of the resin after curing for various periods of time.

low temperatures were used so that the relaxation peaks were located within the frequency window of the dielectrometer. To conduct a frequency-scan test, the sample was cured at 75 °C for a period of time. Then the sample and sensor were removed from the oven and left at room temperature for 20–30 min, during which period the over temperature was cooled to the room temperature. Next the sample and sensor were reinserted into the sealed oven. A constant stream of liquid nitrogen was utilized as a cooling source, and an Omega controller was used to regulate the electric heating to maintain the system at the desired temperature. In each test, the sample was scanned once from high to low frequencies.

Up to 32 frequencies ranging from 10000 to 0.005 Hz were used in the frequency-scan tests. Depending on the low frequencies used, 5–30 min was needed for each scan. These tests may be classified into two groups—those at temperatures below 20 °C and those above 20 °C. For a sample tested below 20 °C, the scans were performed at several temperatures. After each scan, the temperature was raised and a new scan was conducted. For a sample tested above 20 °C, several scans were performed at a constant temperature after the sample was held at the temperature for various periods of time.

Efforts were made to prevent the temperature profiles in the oven/cell of one instrument from deviating from those of the other instruments, and the cure times in different heating environments are considered equivalent.

Results and Discussion

The curing of the epoxy–amine resin was studied using FTIR at temperatures ranging from 55 to 115 °C. Figure 1 shows the IR data. The reaction is slow at the early stages, then accelerates significantly, and finally becomes slow again close to the end of the cure, which is typical of autocatalytic reactions. The glass transition temperature of the resin was measured over the same range of temperature and is shown in Figure 2. The glass transition temperature continues to increase, i.e., the resin continues to cure, even after the resin vitrifies, when the glass transition temperature reaches the cure temperature.

Extraction of Ionic Conductivity and Dipole Relaxation Time. Curing experiments using the microdielectrometer were conducted between 55 and 115 °C. Figure 3 illustrates the dielectric permittivity and the dielectric loss factor obtained during the curing at 115 °C. The permittivity decreases as the cure proceeds and approaches a limiting value at long cure times. The loss factor is high initially and exhibits a peak after the resin cures for approximately 30 min.

The loss factor is composed of two parts—an ionic contribution and a dipole contribution.[11] Since the ionic contribution is independent of frequency, while the dipole contribution is not, the ionic conductivity was extracted

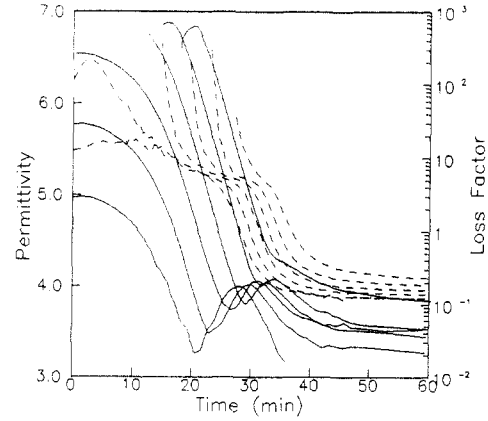

Figure 3. Permittivity (- - -) and loss factor (—) at 115 °C. From left to right, the measurement frequencies are 10000, 1000, 100, 10, 1, and 0.1 Hz.

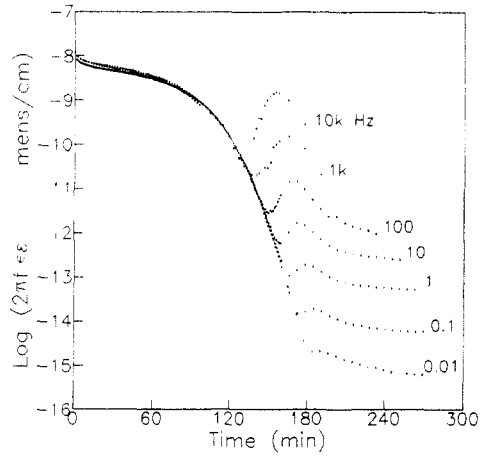

Figure 4. Plot of log ($2\pi fe\epsilon''$) vs cure time for the cure at 75 °C.

from the loss data following a standard method.[12] The loss profiles at various frequencies were transformed into $2\pi fe\epsilon''$ curves (f is the frequency, ϵ'' is the loss factor, and e is the permittivity of free space with a value of 8.85×10^{-12} F/m) and were superimposed to form a single plot. Such a plot is shown in Figure 4 for the resin cured at 75 °C. Over certain periods of time, two or more curves overlap, which indicates frequency independence and negligible dipole contributions. Thus, those experimental data that belong to the overlapped portions of the curves were converted into the ionic conductivity.

Figure 5 is a plot of the ionic conductivity, σ, versus the epoxide conversion at four temperatures. The epoxide

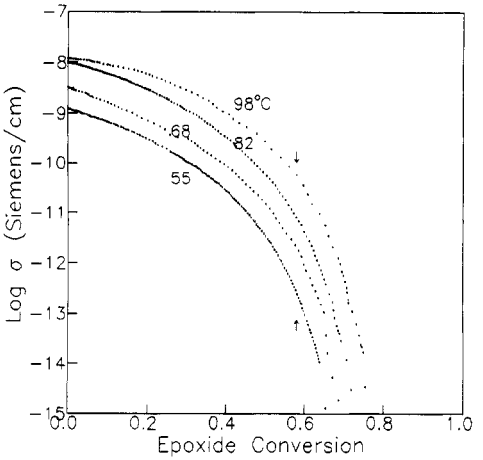

Figure 5. Ionic conductivity vs epoxide conversion. The arrows indicate the gel conversion.

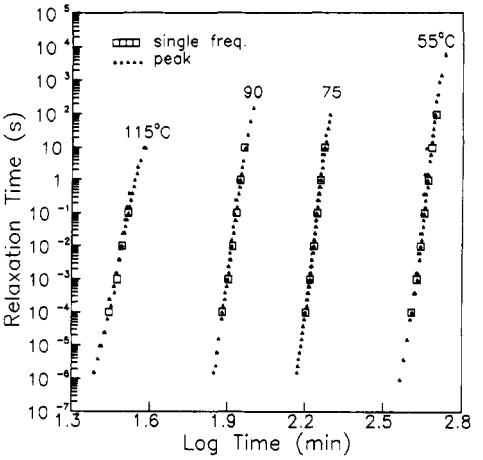

Figure 6. Dipole relaxation times extracted using the single-frequency approach as compared to those obtained directly from the maxima of the loss peaks.

conversions corresponding to the conductivity data were determined using the IR data by linear interpolation. The arrows in the figure indicate the 58% gel conversion of the system evaluated using the recursive approach (assuming equal reactivity of the hydrogen atoms in the diamine).[13,14] The ionic conductivity drops approximately 3 orders of magnitude from the onset of cure to the gel point. With the conductivity and the conversion data, the overall diffusion coefficient of the molecular species in the pregel stage was estimated using the diffusion model:[6]

$$D = \frac{K_2}{K_1}\sigma\bar{x}_n^{-1} \tag{3}$$

where D is the overall diffusion coefficient or the average diffusion coefficient of a monomer unit, K_1 and K_2 are constants for isothermal cure, and $\bar{x}_n$ is the number-average degree of polymerization. Because the constants, K_1 and K_2, are unknown, the diffusion coefficient obtained was normalized with respect to the value at 0% conversion. For the epoxy–amine resin, $\bar{x}_n = 1/(1 - 4\alpha/3)$ by assming no cycle formation[13] and its value at the gel conversion is only about 4 times the value at 0% conversion. Thus, the ionic conductivity changes much faster than the other three factors (K_1, K_2, and $\bar{x}_n$) in the model and is the dominating factor.

The dipole relaxation time may be directly obtained from the maxima of the dipole loss peaks, such as those in Figure 3, by evaluating the cure times at which the maxima are reached. The inverse frequency is the relaxation time at the particular cure time. Thus, each frequency used in the experiment yields only a single relaxation time. By following a single-frequency approach based on the work of Mangion and Johari,[15] many more relaxation data have been obtained for the epoxy resin.[16] This method includes the following steps: (i) fitting the complex permittivity obtained with a single frequency during isothermal cure to a modified Williams–Watts relaxation function; (ii) evaluating the relaxation time of the Williams–Watts function corresponding to each of the permittivity data; and (iii) converting the Williams–Watts relaxation time to the dipole relaxation time.

Figure 6 shows the dipole relaxation time obtained from the two methods. The data determined using the single-frequency approach are in agreement with those obtained directly from the loss peaks but cover a much wider range. These data were utilized to estimate the post gel diffusivity based on the free-volume relationship:[6]

$$D\tau^n = K_3 \tag{4}$$

where n, the power-law index, is a constant independent of conversion and temperature and K_3 is a constant.

Determination of the Power-Law Index *n*. Equation 4 is useful only when the power-law index n is known. Substituting eq 3 into eq 4 and rearranging yields

$$\log(\sigma\bar{x}_n^{-1}) = -n \log \tau + \log K_3' \tag{5}$$

where K_3' ($=K_1K_3/K_2$) is a constant. Thus, n may be obtained by determining both the diffusion coefficient and the relaxation time over the same stages of cure, e.g., in the pregel stage.

The frequency-scan tests were conducted at temperatures ranging from −11.1 to 40 °C to measure the ionic conductivities and dipole relaxation times of pregel samples. DSC experiments indicate that the samples were typically scanned at temperatures at least 10 °C above the corresponding glass transition temperatures. For the tests below 20 °C, the samples were cured at 75 °C for up to 100 min and scanned at 4 or 5 temperatures with a 4.4 °C increment. Figure 7 shows the loss factor measured during scans at −4.4, 0.0, 4.4, and 8.9 °C for a sample cured at 75 °C for 60 min. The dipole loss peaks are located at relatively high frequencies and the ionic contribution is evident at low frequencies. At relatively high temperatures (4.4 and 8.9 °C), the dipole losses were negligible at low frequencies and the data were used to determine the ionic conductivity. For a sample tested above 20 °C, several scans were conducted while the sample was kept at a constant temperature. Because the scan temperatures were relatively high, significant changes in the dielectric data were observed for the samples kept for different periods of time. Figure 8 shows the loss factor measured at 31.1 °C after curing at 75 °C for 99 min. The ionic conductivity was calculated using the low-frequency loss data with negligible dipole contributions. The dipole relaxation time was evaluated by locating the maxima of the dipole loss peaks; the detailed procedure has been given elsewhere.[16]

The epoxide conversions of the samples scanned below 20 °C were found to range from 0 to 34%, which were the IR conversions after the curing at 75 °C. For the samples scanned above 20 °C, the epoxide conversions were between 31 and 48%, which were IR conversions at the beginning of each scan and were obtained from the IR experiments that followed the same test schedules as those of the scanned samples. Because the time taken in each fre-

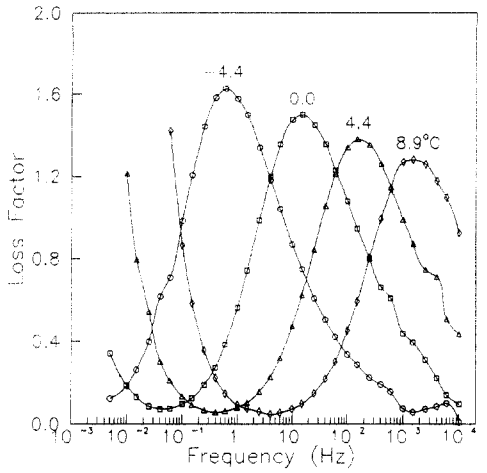

Figure 7. Loss factor for a sample cured at 75 °C for 60 min.

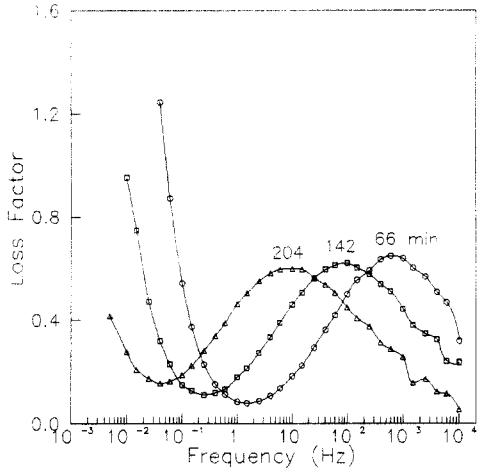

Figure 8. Loss factor (O) at 31.1 °C. The sample was cured at 75 °C for 99 min and then kept at 31.1 °C for various periods of time.

quency-scan test was short and the reaction was slow, any reaction during the dielectric measurements was not considered. Based on the sample conversion, the number-average degree of polymerization $\bar{x}_n$ was then calculated by assuming no cycle formation.

The above results allowed construction of the plot of the diffusion coefficient ($\sigma\bar{x}_n^{-1}$) vs the dipole relaxation time for the pre gel samples. Such plots are shown in Figure 2 of ref 6 for nine temperatures. The data at each temperature exhibit linear dependence and the best linear correlations form parallel lines. This result is consistent with eq 5. The average slope of the lines was −0.81, indicating n = 0.81.

Cure-Dependent Diffusion and Diffusion-Controlled Kinetics. The above results were then used to estimate the diffusion coefficient of the epoxy–amine resin. Figure 9 is a plot of the normalized diffusion coefficient ($D/D_{\alpha=0}$) versus the cure time. For the pregel stage, the data (shown by the open circles) were obtained using the diffusion model, eq 3, by assuming no cycle formation so that $\bar{x}_n = 1/(1-4\alpha/3)$. In the postgel stage, the data shown by the open triangles were calculated using the free-volume relationship, eq 4. Because the range of frequencies covered by the dielectrometer is limited, at a relatively high temperature, e.g., 82 or 115 °C in the figure, the shortest dipole relaxation time was obtained in the postgel stage; i.e., a gap was created between the range of conversions covered by eq 3 and that covered by eq 4. In such cases, the diffusion coefficient close to the gel

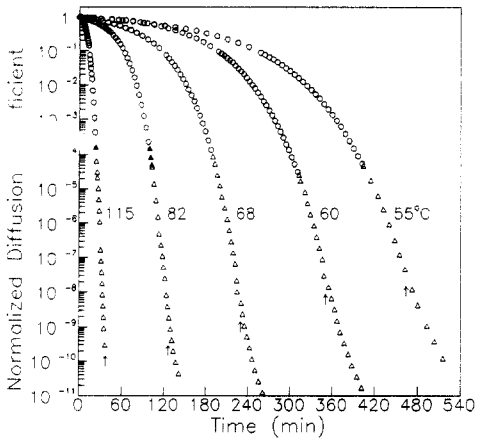

Figure 9. Normalized diffusion coefficient vs cure time: (O) eq 3; (▲) eq 4; and (△) eq. 6. The arrows indicate the vitrification times.

conversion was estimated by neglecting the contribution of the gel. Since the diffusion coefficient of starlike polymers is much smaller than that of linear chains[17] and the gel fraction is small close to the gel point, the diffusion in the cure system is dominated by the diffusion of the sol and the gel contribution may be neglected.[6] Therefore

$$D = w_s D_s = \frac{K_2}{K_1}\sigma\bar{x}_{ns}^{-1}w_s \tag{6}$$

where D_s is the diffusion coefficient of the sol, w_s is the weight fraction of solubles, and $\bar{x}_{ns}$ is the number-average degree of polymerization of the sol. In this work, both w_s and $\bar{x}_{ns}$ were calculated based on the recursive approach[13,14] (see Appendix). The normalized diffusion coefficient obtained using eq 6 is shown by the closed triangles in Figure 9. The weight fraction of solubules involved in the calculations was always larger than 50%.

Figure 9 illustrates how the diffusivity changes as the liquid resin is transformed into a glassy material. The vitrification times of the resin are shown by the arrows. As the cure proceeds, the diffusion coefficient decreases monotonically. Immediately after the onset of the cure, the decline is small since the autocatalytic reaction is slow and the main product of the polymerization is oligomers. As the reaction accelerates, the diffusion coefficient starts to decrease rapidly. The evolution of the structure of the resin from a system of monomers and oligomers to one with a growing network also contributes to the decline of the diffusivity. After vitrification, the reaction is much slower based on the IR data but the diffusivity continues to drop. Depending on the cure temperature, the normalized diffusion coefficient decreases by 7–10 orders of magnitude before the system reaches the glassy state.

The normalized diffusion coefficient is plotted against the epoxide conversion in Figure 10. At low conversions, when condensation of monomers and oligomers is the major curing event, the diffusion coefficient decreases slowly. Starting from close to the gel point when chain branching and cross-linking dominate, the diffusion coefficient decreases rapidly even for a small advancement of the reaction. This indicates that the diffusivity is very sensitive to the structural changes, the network formation and growth, of the system. It is also evident from Figure 10 that the relationship between the normalized diffusion coefficient and conversion is temperature dependent—the diffusivity exhibits higher conversion dependence at a low temperature than at a high temperature. This is because the diffusion coefficient, a transport property, is dependent

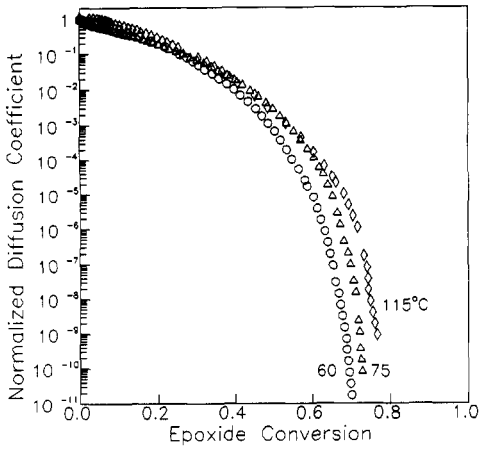

Figure 10. Conversion dependence of the normalized diffusion coefficient.

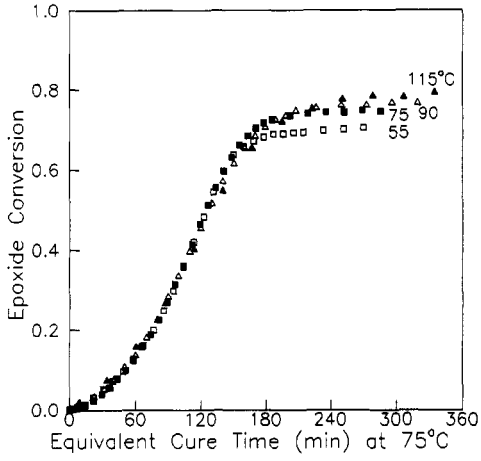

Figure 11. Epoxide conversion vs equivalent cure time at 75 °C.

on the free-volume of the system or the difference between the cure temperature and the glass transition temperature.

To compare the normalized diffusion data to those predicted by the existing models, the cure kinetics needs to be examined first.

One way to detect the diffusional effects on the reaction kinetics is to superimpose the kinetic data or the glass transition temperatures obtained at various cure temperatures.[18,19] If a reaction is kinetically controlled, the Arrhenius rate expression may be written as

$$\frac{d\alpha}{dt} = k_0 \exp\left(-\frac{E_a}{RT}\right) g(\alpha) \tag{7}$$

where E_a is the activation energy, k_0 is a constant, and g is a function of conversion. Integrating this equation yields

$$G(\alpha) = \ln k_0 - \frac{E_a}{RT} + \ln t \tag{8}$$

where $G = \mathrm{Ln}(\int d\alpha/g)$. Now, if the kinetic data at various temperatures are shifted by $(-E_a/RT)$, the data should form a master curve on the α–t plot. This is also true for the glass transition temperature on the T_g–t plot since there exists a one-to-one relationship between conversion and glass transition temperature. The diffusional effect may be detected when the data at one temperature deviate from the master curve.

In Figures 11 and 12, the α–t and T_g–t curves of various temperatures are horizontally shifted to superimpose with the curves at 75 °C. To determine the shifting factor for an α–t and T_g–t curve, the equivalent cure time at 75 °C

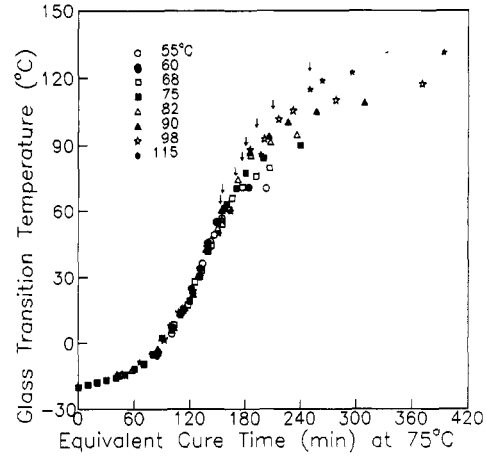

Figure 12. Glass transition temperature vs equivalent cure time at 75 °C. The arrows indicate the equivalent vitrification times.

was calculated for each epoxide conversion or glass transition temperature in the pregel stage. Then, a univariable search was conducted to minimize the differences between the actual cure times at 75 °C and the equivalent cure times and the shifting factors were calculated. The gel time at 75 °C was found to be 138 min when the IR conversion reached the 58% gel conversion. It is seen from the two figures that the curves overlap at cure times shorter than the gel time, demonstrating that the effect of diffusion on the reaction kinetics is unimportant in the pregel stage. Significant divergences of the curves becomes evident about 20 min after the gel time, indicating that the diffusional limitations are affecting the cure kinetics. The onset of the deviation of one curve from the master curve is more easily detected on the T_g plot than on the conversion plot. The vitrification times are also shown in Figure 12. The onsets of the deviations approximately coincide with the vitrification times.

Since the effect of diffusion on the cure kinetics is insignificant in the pregel stage, the pregel kinetic data were then utilized to evaluate the intrinsic rate constants. The IR data were fitted to the rate equation, eq 1, and k_p and k_i were determined for each cure temperature. The activation energy and the frequency factor were 48.8 kJ/mol and 8.72×10^5 min^{-1} for k_p and 63.2 kJ/mol and 2.16×10^6 min^{-1} for k_i.

The cure-dependent diffusion of epoxy amine resins has been modeled by Huguenin and Klein based on the free-volume theory:[7]

$$D = D_0 \exp\left\{b_D\left[1 - \frac{1}{f_g + \beta_f(T - T_g)}\right]\right\} \tag{9}$$

where D_0 and b_D are constants, f_g is the fractional free volume at T_g, and β_f is the thermal expansion coefficient of the free volume.

In this work, the two constants, D_0 and b_D, were determined following a procedure similar to the one used in ref 7. The diffusional limitations to the cure kinetics were evaluated using the Rabinowitch model:[9]

$$\frac{1}{k} = \frac{1}{k_c} + \frac{1}{k_{d0}D} \tag{10}$$

where k is the diffusion-corrected rate constant, k_c is the intrinsic rate constant, and k_{d0} is another constant. Since k_p in eq 1 is the rate constant of the major polymerization

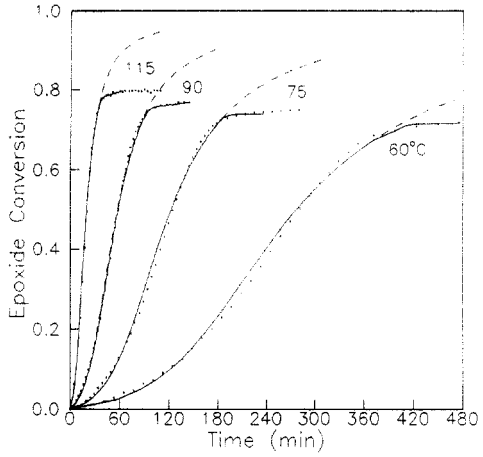

Figure 13. FTIR and model conversion curves for various cure temperatures: (···) experiments; (– – –) intrinsic kinetic model, eq 1; (—) diffusion-controlled model, eq 11, based on ref 7.

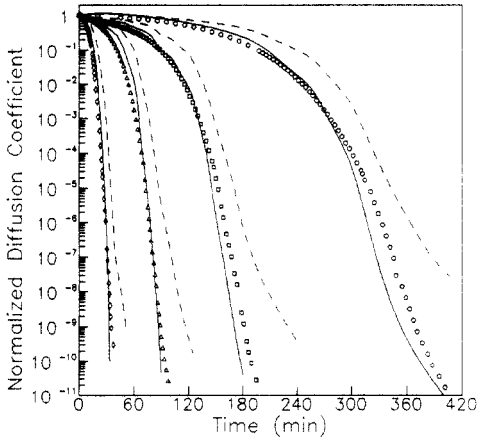

Figure 14. Comparison of the normalized diffusion coefficients obtained using different methods. From left to right, the cure temperatures are 115, 90, 75, and 60 °C: (○,□,△,◇) the proposed approach; (—) free-volume model; (– – –) cooperative rearrangement model.

reaction, the diffusion-controlled kinetic model was formulated as

$$\frac{d\alpha}{dt} = \left(\frac{1}{k_p} + \frac{1}{k_{d0}D}\right)^{-1}\left(\alpha + \frac{k_i}{k_p}\right)(1-\alpha)(r-\alpha) \qquad (11)$$

This model was used to fit the kinetic data to determine b_D and $k_{d0}D_0$. f_g was taken as 0.025. β_f was 4.8×10^{-4} K^{-1} for $T_g < T < T_g + 100$ and 4.8×10^{-5} K^{-1} for $T < T_g$.[7,20] The glass transition temperatures were those obtained from the DSC tests. As Figure 13 indicates, the kinetic data are well fitted by this diffusion-control model, eq 11. The values of b_D obtained for all the cure temperatures were then used to evaluate the diffusion coefficient using the free-volume model, eq 9.

Another diffusion model was based on the Adam–Gibbs theory of cooperative rearrangement,[8] which is given by

$$D = D_0 \exp\left[-\frac{m}{T\ln\left(\frac{T}{T_g - 50}\right)}\right] \qquad (12)$$

where D_0 and m are constants. For polymers, m is typically 10^3 K. This value was also used in the present calculations.

Figure 14 illustrates the normalized diffusion coefficients obtained from the three methods. The diffusion coefficient determined using the newly developed approach is in agreement with that of the free-volume model. Both

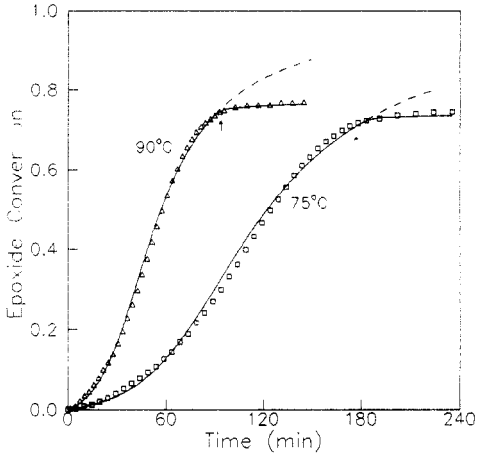

Figure 15. FTIR kinetic data vs the model predictions: (□,△) IR data; (– – –) intrinsic kinetic model, eq 1; (—) diffusion-controlled kinetic model, eq 13. The arrows indicate the vitrification times.

methods predict the same trend of the cure dependence of the diffusion coefficient. The difference between the two predictions is not significant considering the accuracy of the data from the free-volume model. The diffusion coefficient from the cooperative rearrangement model disagrees with those from the other two approaches and exhibits considerably slower decline with respect to the cure time. The discrepancy may be due to one of the assumptions made in the derivation of the cooperative rearrangement model. The assumption states that the discontinuity of the isobaric heat capacity at glass transition ΔC_p is independent of conversion.[8] But, for the epoxy–amine resin studied, ΔC_p decreases gradually during cure; its value for the fully cured sample was found to be less than half of the value of the uncured sample. Since the diffusion coefficient is an exponential function of m by eq 12 and m is inversely proportional to ΔC_p, the diffusion coefficient is an exponential function of $1/\Delta C_p$. The decrease of ΔC_p may have caused the observed discrepancy in the model predictions.

The normalized diffusion coefficient obtained from the newly developed approach was also used to model the cure kinetics of the epoxy–amine resin. The Rabinowitch model, eq 10, which governs the diffusion-controlled kinetics of small-molecule reactions, has been employed in a number of studies involving reactions between polymers.[7,8,21] In this work, the diffusion-controlled kinetic model for the epoxy resin was also constructed based on the Rabinowitch model. Again, since k_p is the rate constant of the major polymerization reaction, the diffusional effect is scaled with respect to k_p to yield the following model:

$$\frac{d\alpha}{dt} = \left(\frac{1}{k_p} + \frac{1}{k_{d0}'\dfrac{D}{D_{\alpha=0}}}\right)^{-1}\left(\alpha + \frac{k_i}{k_p}\right)(1-\alpha)(r-\alpha) \qquad (13)$$

where $D/D_{\alpha=0}$ is the normalized diffusion coefficient and k_{d0}' ($=k_{d0}D_{\alpha=0}$) is a constant. Thus, there is only one new constant in eq 13, which is due to the constant k_{d0} in the Rabinowitch model. The newly developed approach has not introduced extra adjustable constants into the diffusion-controlled kinetic model. With the intrsinic rate constants known, a univariable search was conducted to fit the experimental kinetic data to eq 13.

Figure 15 shows the conversion profiles of the diffusion-controlled kinetic model for the curing at 75 and 90 °C, respectively. The experimental kinetic data are in agree-

ment with the model predictions. The curing reaction becomes significantly slower close to vitrification. Starting from the same period, the rate of reaction predicted by the intrinsic kinetic model is too large as compared to the experimental data. The diffusion-controlled kinetic model, however, shows continued but decelerated reactions rather than fast reaction or cessation of the curing. By altering the apparent rate constant, this model successfully predicts the deceleration of reactions due to the diffusional limitations, which also demonstrates that the Rabinowitch model and the diffusion coefficient obtained following the newly developed approach are useful in modeling the overall cure kinetics.

Depending on the cure system and the processing conditions, the diffusion control may occur at different stages. To accurately control the end properties of the resin and to completely characterize its processability, it is of practical importance to construct a quantitative kinetic model that is valid over the entire range of cure. The current modeling approach forms the basis for the study of the overall cure kinetics and the optimization of the processing conditions of thermosetting resins.

Conclusions

The molecular diffusion during the curing of the epoxy–amine resin was characterized following the approach based on the dielectric analysis.[6] The diffusion coefficient was estimated using the diffusion model, eq 3, and the free-volume relationship, eq 4, by measuring the ionic conductivity and dipole relaxation time of the resin. From the onset of cure to vitrification, the diffusivity in the resin system decreases by 7–10 orders of magnitude depending on the cure temperature. At low conversions, when condensation of monomers and oligomers prevails, the diffusivity decreases slowly, whereas, at higher conversions, when chain branching and cross-linking dominate and, later, the infinite network forms and grows, the diffusion coefficient drops quickly for even a small increment in conversion. Such a trend continues into the postvitrification stage. Thus, the diffusivity is highly sensitive to the structural changes in the system.

The estimated normalized diffusion coefficient is in agreement with the predictions of the free-volume model. The predictions of the cooperative rearrangement model exhibit slower decline of the diffusivity. This discrepancy was attributed to the changing ΔC_p at T_g during cure since a small change in ΔC_p may lead to large fluctuation in the predicted diffusion coefficient.

A diffusion-controlled kinetic model was established based on the Rabinowitch model of small-molecule reactions and the normalized diffusion coefficient obtained from the newly developed approach. This kinetic model predicted continued but decelerated reactions starting from the vicinity of vitrification and was found to fit the experimental conversion profiles well. The current findings form the basis for the control and optimization of the processing conditions of thermosetting systems.

Acknowledgment. The highly purified epoxy resin was supplied by Shell Development Co.

Appendix

The polymerization of the epoxy–amine resin is an A_4–B_2 copolymerization, where A corresponds to an amine hydrogen and B an epoxide. For a stoichiometrically balanced system ($r = 1$), the weight fraction of solubles is[14]

$$\omega_s = \frac{M_{A_4}}{M_{A_4} + 2M_{B_2}} P(F_A^{out})^4 + \frac{2M_{B_2}}{M_{A_4} + 2M_{B_2}} P(F_B^{out})^2 \quad \text{(A1)}$$

where M_{A_4} and M_{B_2} are the molecular weights of the diamine and the diepoxide and $P(F_A^{out})$ and $P(F_B^{out})$ retain the same meanings as those in ref 14.

By assuming no cycle formation in the solubles, the number-average degree of polymerization is simply

$$\bar{x}_{ns} = \frac{\bar{M}_{ns}}{\bar{M}_n(p=0)} = \frac{M_{A_4} + \frac{2}{r_s} M_{B_2}}{1 + \frac{2}{r_s} - 4\frac{p_{B_s}}{r_s}} \frac{3}{M_{A_4} + 2M_{B_2}} \quad \text{(A2)}$$

where $\bar{M}_n$ is the number-average molecular weight, $\bar{M}_{ns}$ is the number-average molecular weight of the sol, p is the extent of reaction, p_{Bs} is the extent of reaction of epoxides in the sol which is equivalent to the epoxide conversion of the sol, and r_s is the stoichiometric ratio of the sol. Note that $\bar{x}_{ns}$ is defined with respect to $\bar{M}_n(p=0)$, or the average molecular weight of the monomers. This is because $\bar{x}_{ns}$ represents the ratio of the diffusion coefficient at certain conversion to the diffusion coefficient of monomer.

r_s and p_{B_s} may be written as[22]

$$r_s = \frac{P(F_A^{out})^4}{P(F_B^{out})^2}, \qquad p_{B_s} = \frac{P(F_A^{out})^3 p}{P(F_B^{out})} \quad \text{(A3)}$$

References and Notes

(1) Bell, J. P. *J. Polym. Sci., Part A-2* **1970**, *8*, 417.
(2) Sourour, S.; Kamal, M. R. *Thermochim. Acta* **1976**, *14*, 41.
(3) Dušek, K.; Ilavský, M.; Luňák, S. *J. Polym. Sci., Polym. Symp.* **1975**, *53*, 29.
(4) Prime, R. B.; Sacher, E. *Polymer* **1974**, *13*, 455.
(5) Rozenberg, B. A. *Adv. Polym. Sci.* **1986**, *75*, 113.
(6) Deng, Y.; Martin, G. C. *Macromolecules*, preceding paper in this issue.
(7) Huguenin, F. G. A. E.; Klein, M. T. *Ind. Eng. Chem., Prod. Res. Dev.* **1985**, *24*, 166.
(8) Havlíček, I.; Dušek, K. In *Crosslinked Epoxies*; Sedláček, B., Kahovec, J., Eds.; Walter de Gruyter: Berlin, 1987.
(9) Rabinowitch, E. *Trans. Faraday Soc.* **1937**, *33*, 1245.
(10) ASTM D1652-90.
(11) Senturia, S. D.; Sheppard, N. F., Jr. *Adv. Polym. Sci.* **1986**, *80*, 1.
(12) Day, D. R. *Polym. Eng. Sci.* **1986**, *26*, 362.
(13) Macosko, C. W.; Miller, D. R. *Macromolecules* **1976**, *9*, 199.
(14) Miller, D. R.; Macosko, C. W. *Macromolecules* **1976**, *9*, 206.
(15) Mangion, M. B. M.; Johari, G. P. *J. Polym. Sci., Polym. Phys. Ed.* **1990**, *28*, 1621; **1991**, *29*, 1127.
(16) Deng, Y.; Martin, G. C., accepted for publication in *J. Polym. Sci., Polym. Phys. Ed.*
(17) Bartels, C. R.; Crist, B.; Fetters, L. J.; Graessley, W. W. *Macromolecules* **1986**, *19*, 785.
(18) Luňák, S.; Vladyka, J.; Dušek, K. *Polymer* **1978**, *19*, 931.
(19) Simon, S. L.; Wisanrakkit, G.; Gillham, J. K. *Polym. Mater. Sci. Eng.* **1989**, *61*, 799.
(20) Bravenec, L. D. Ph.D. Dissertation, University of Delaware, 1983.
(21) Rohr, D. F.; Klein, M. T. *Ind. Eng. Chem. Res.* **1988**, *27*, 1361; **1990**, *29*, 1210.
(22) Miller, D. R.; Valles, E. M.; Macosko, C. W. *Polym. Eng. Sci.* **1979**, *19*, 272.